AD NUMBER

AD430590

NEW LIMITATION CHANGE

TO

Approved for public release, distribution unlimited

FROM

Distribution authorized to U.S. Gov't. agencies and their contractors; Administrative/Operational Use; FEB 1964. Other requests shall be referred to Commanding Officer, Army Biological Laboratories, Frederick, MD 21701.

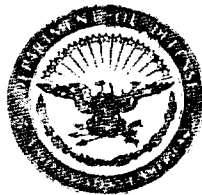AUTHORITY

NTIS, BDRL D/A ltr, 27 Sep 1971

UNCLASSIFIED

AD 430590

DEFENSE DOCUMENTATION CENTER

FOR

SCIENTIFIC AND TECHNICAL INFORMATION

CAMERON STATION, ALEXANDRIA, VIRGINIA

TECHNICAL MANUSCRIPT 109

MODELS FOR DEAGGLOMERATION
AND FRACTURE
OF PARTICULATE SOLIDS

FEBRUARY 1964

DDC
MAR 3 1964
TISIA D
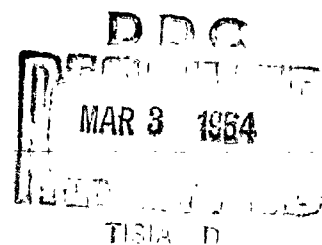
UNITED STATES ARMY
BIOLOGICAL LABORATORIES
FORT DETRICK

U.S. ARMY BIOLOGICAL LABORATORIES
Fort Detrick, Frederick, Maryland

TECHNICAL MANUSCRIPT 109

MODELS FOR DEAGGLOMERATION AND FRACTURE OF PARTICULATE SOLIDS

John S. Derr, Jr.

Physical Sciences Division
DIRECTOR OF BIOLOGICAL RESEARCH

1

2

The work reported here was performed under
Project 4B11-02-068, "Physical and Chemical
Studies of Biological Agents," Task -02,
"Chemical and Biophysical Changes in BW
Agents Induced by Environmental Stresses."
This material was originally submitted as
manuscript 5245.

The information in this document has not been cleared for
release to the public.

DDC AVAILABILITY NOTICE

ABSTRACT

Models for deagglomeration of aggregates of particles by compressible flow systems and for the fracture of particles by impact grinding have been developed, leading to a prediction of particle-size distributions, i.e., quasi-logarithmico-normal distributions, with a mean geometric standard deviation of 1.6 ± 0.1.

For aerodynamic deagglomeration, the size distribution is related to the compressible flow properties and intrinsic properties of the particulate solids. Impact grinding is shown to be governed by impact probabilities proportional to the square of the Stokes' equivalent spherical particle diameter. Data are presented in support of the models, and departures from the models are discussed.

CONTENTS

FIGURES

6

TABLES

I.   INTRODUCTION

The aerosol generation of particulate solids consists either of fracturing larger particles and creating an air dispersion of their fragments, or of separating preformed particles held together in aggregates by surface contact or other forces. In the first case, new surface area is created, requiring in general larger expenditures of energy and applications of larger stresses. Concomitant with the exposure of fresh surface to the gaseous environment, opportunity for catalysed chemical reactions is afforded, which could shift the powder into a non-equilibrium condition. Because of the relatively high energy and stress requirements for increasing surface area, aerosols of powders are usually generated from a pre-sized product, prepared either by grinding or spray drying. Special techniques do exist, however, for the preparation of certain dry materials that make possible the stable aerosol generation of non-presized powders, through reduction of stress required in the creation of new surface by alteration of powder properties.

In general, however, any particulate solid aerosol generation process involves both the creation of fresh surface, or grinding, and the separation of basic presized particles held together as aggregates, or deagglomeration. The relative extent of grinding and deagglomeration depends upon the energy available in the generating system as well as its compressible flow characteristics, the particle-size distribution of the pre-dispersed powder, the design of the aerosol generating mechanism, and the intrinsic physical properties of the solid medium comprising a particle.

The purpose of this paper will be to present models for grinding, and for particulate solid aerosol generation involving compressible fluid dynamics, in an attempt to correlate properties of the generating systems and the pre-dispersed powder, hopefully leading to a prediction of the initially generated aerosol size distribution. Modification of the initial aerosol distribution by coagulation, preferential sedimentation or diffusion, etc., will not be discussed.

II. AERODYNAMIC DEAGGLOMERATION OF PARTICULATE SOLIDS

A. CONFORMATION OF AN AGGREGATE

In the discussion which follows, it will be assumed that the basic
particles comprising the powder are homogeneous in size, a basic particle
being defined as the smallest volumetric subdivision of the powder possible
without the creation of fresh surface. This assumption does not strictly
apply to most powders dealt with experimentally, but if geometric standard
deviations of the distributions are small the assumption does not introduce
any serious error. A proper statistic, such as Sauter Mean diameter, aver-
age volume diameter, area mean diameter, etc., can be chosen to approximate
an equivalent "homogeneous size" for a given application.

It will be further assumed that the basic particles are initially
separated from each other, i.e., no aggregates are initially present, and
that they are in random motion with respect to each such as applies to a
turbulent gas suspension or to a mechanically stirred array. Random motion
will produce collisions, collisions will produce aggregates, and a steady
state will be reached when deagglomerating forces brought to bear on an
aggregate are equal to forces of cohesion holding the aggregate together.
Aggregates consisting of various numbers of basic particles can be formed
in two limiting ways:

1. Type 1

Type 1 results from random collisions between basic particles
simultaneously in every volume element of the array, and continuing
collisions between resulting aggregates, etc. Non-uniform packing of
basic particles results.

2. Type 2

Type 2 is caused by the initial formation of an agglomerate by
collision of two basic particles, and successive build-up of this
agglomerate by successive collisions between it and individual basic
particles. Uniform packing of basic particles results.

A schematic representation of agglomerate formation in both models,
assuming collisions between two particles for illustration, is given in
Figure 1.

Type 1

Number Basic Particles in Agglomerate, Ni	Array	Array Index	Probability of Agglomerate Configuration
1		0	
2		1	$P_c < 1$
4		2	P_c^2
8	etc.	3	P_c^3

Type 2

1		0	
2		1	$P_c < 1$
3		2	P_c^2
4		3	P_c^3
5	etc.	4	
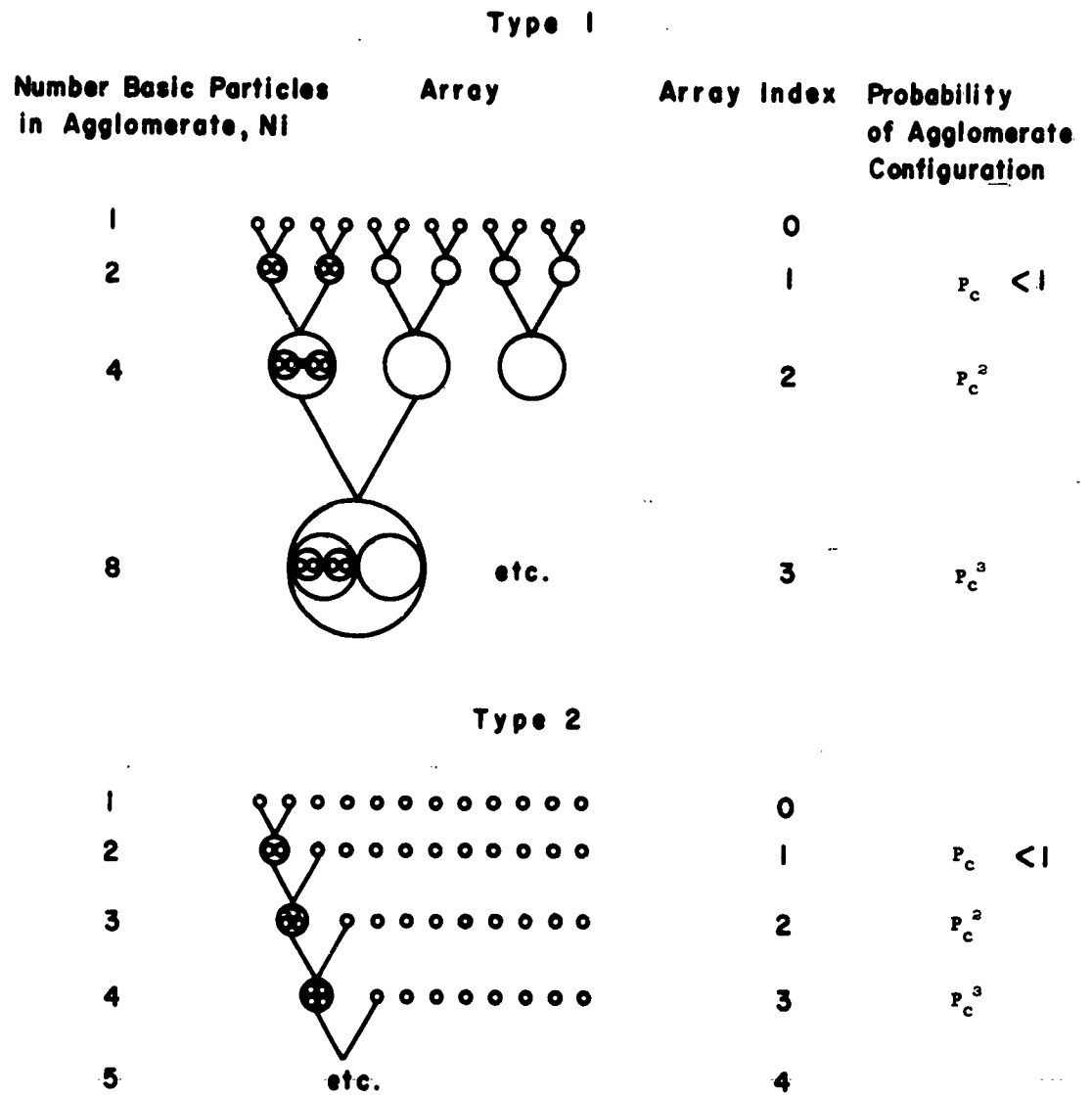
Figure 1. Limiting Types of Agglomerate Formation.
(Two-Particle Collision Assumed.)

If $\tilde{P}_c$ is the probability of a single collision involving two particles, taken as equal for both models, then the probability of forming an agglomerate consisting of N_i basic particles for each type is:

$$\tilde{P}_{(N_i)_1} = \tilde{P}_c^{\left(\frac{\log_{10} N_i}{0.301}\right)} \tag{1}$$

where $N_i = 2^i$

i = array index

$$\tilde{P}_{(N_i)_2} = \tilde{P}_c^{\left(N_i - 1\right)} \tag{2}$$

The ratio of probabilities of forming an agglomerate of type 1 to type 2 consisting of the same number of particles is then

$$R = \frac{\tilde{P}_{(N_i)_1}}{\tilde{P}_{(N_i)_2}} = \tilde{P}_c^{\left(\frac{\log N_i}{0.301} + 1 - N_i\right)} \tag{3}$$

Since $\tilde{P}_c < 1$, it is seen that aggregates formed by the mechanism of type 1 are much more probable than those of type 2. For example for $\tilde{P}_c = 0.5$ and $N_i = 8$, then $R = 16$; or $\tilde{P}_c = 0.2$, $N_i = 8$ then $R = 625$. As $\tilde{P}_c$ decreases, or N_i increases, R increases.

Hence, the conformation of what might be considered a most probable or representative agglomerate will be that determined by probabilities associated with type 1, having:

(1) a quasi-spherical shape, due to the spherical symmetry of random motion of colliding particles.

(2) five sub-agglomerate components, on the average being the smallest number of colliding particles defining the spherical symmetry. Each of these component sub-agglomerates will consist of five smaller sub-agglomerates, etc., ending with a sub-agglomerate consisting of five basic particles, which would correspond to the first aggregate formed in the initially dispersed random array.

A schematic diagram of this hypothetical characteristic aggregate is shown in Figure 2.
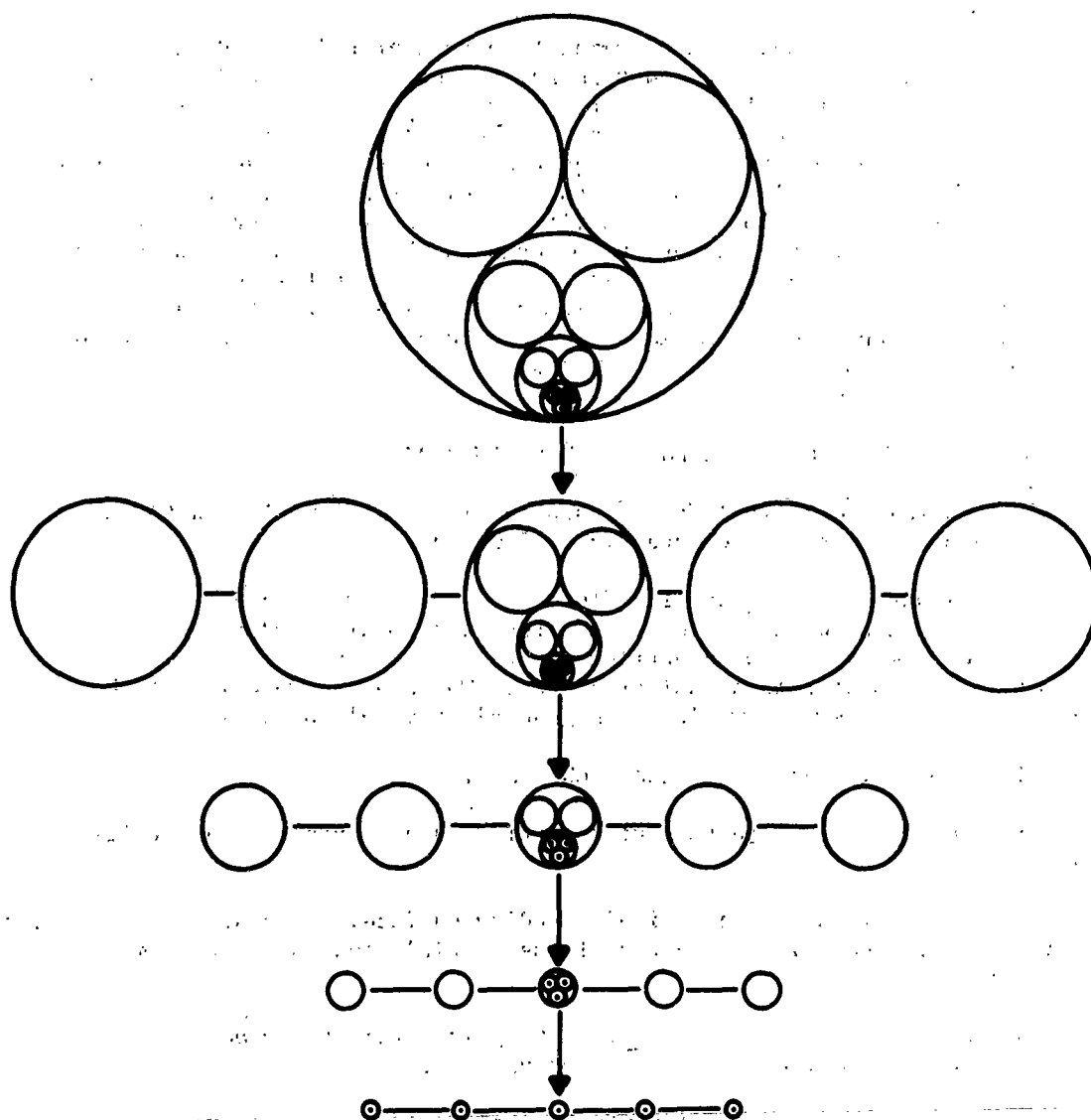
Figure 2.   Cross-Section Schematic of "Probable" Quasi-Spherical
Agglomerate and Mechanism of Deagglomeration.

12

The largest characteristic aggregate encountered in a bed of pre-dispersed powder will be that determined by the magnitude and efficiency of application of the disrupting stress during the powder's history, schematically represented in Figure 2. The process of aerosol generation then can be considered as a sequential process of breaking an agglomerate of type 1 into its component sub-agglomerates, etc., until either stable sub-agglomerate or basic particles are dispersed. An important property of the sub-agglomerate hypothesis is the decrease in numbers of contacts per unit area between component particles as the agglomerate increases in size, i.e., as the agglomerate gets larger, its shear strength or tensile strength gets smaller. This would not be the case for agglomerates of type 2 formation.

B. DISRUPTION OF AGGLOMERATES BY AERODYNAMIC DRAG

In general, mechanical forces capable of deagglomerating particles arise in seven ways in a compressible flow system:

1. Impact of particles with fluid flow boundary walls due to vorticity of the particles' motion. This could result from high-order turbulence in the fluid flow system, or centrifugal force applied to a particle as a result of its motion in a laminar vortex. The average velocity of the particle in this system would be in general parallel to the impact surface.

2. Impact of particles with each other.

3. Centrifugal disruption of a particle due to rotation about its own axis.

4. Direct impact with a fixed bounding surface, not requiring vorticity, where the average velocity vector of the particle intersects the impact surface.

5. Friction drag, or shear, resulting from velocity gradients in a viscid fluid system; and form drag, or pressure.

6. Inertia, causing preferential acceleration by drag forces acting unevenly over particles in contact and composing an aggregate.

7. Explosive decompression of an agglomerate containing trapped air in its voids if surface pressure is rapidly reduced. This effect can theoretically exist for a spherical agglomerate under drag in a free stream.

For the interaction of a free, unbounded gas stream and a particle, mechanisms (5), (6) and (7) would predominate. Drag includes both a pressure stress and a shear stress, and for a sphere in steady laminar flow of a viscous incompressible medium, or for a compressible medium

at Mach $\leq$ 0.3, these stresses are normal to each other and normal and parallel to the surface respectively.[1] The resultant drag force under these conditions is parallel to the direction of motion, and is given by Stokes' law for spheres with radii $> 1\mu$. [The Cunningham correction factor to account for slip is required for radii $< 1\mu$.]

$$D_s = 6 \pi \eta U r \qquad (4)$$

U = relative stream-particle velocity

r = radius of sphere, or characteristic dimension

η = viscosity of medium

Stokes' equation holds for laminar flow, which, for a sphere, requires a Reynolds number, $R_e \leq 1$

$$R_e = \frac{\rho U r}{\eta} \leq 1 \qquad (5)$$

ρ = density of medium

A general expression for the drag or resultant force on a particle of any shape in either incompressible or compressible media for either turbulent or laminar flow has been formulated in terms of a drag coefficient. Drag acts on a particle in direction of relative motion of the medium with respect to the particle.

$$D = \frac{C_D \rho U^2 S}{2} \qquad (6)$$

U = free stream velocity

S = projected area of body normal to stream

C_D = drag coefficient

ρ = density of medium at particle surface

The drag coefficient is a function of shape and Reynolds number, and for irregular shapes is empirically determined.[2] A function relating C_D and R_e for spheres over the range of $0 \leq R_e \leq 2000$ has been derived by Langmuir[3] with average deviations from experimentally determined values of less than 4 per cent.

$$C_D \, R_e/24 = 1 + 0.197 \, R_e^{0.63} + 2.6 \times 10^{-4} \, R_e^{1.38} \tag{6)A}$$

If a particle is free to conform to an external pressure stress over its surface, its shape will be altered if the resultant stress is not uniform in magnitude and direction over every region of the surface. It can be shown that particles obeying Stokes' law are not distorted. However, particles accelerated in compressible media do experience non-uniform as well as non-symmetrical pressure stresses, and aggregates of particulate solids or liquid droplets will deform during acceleration if the magnitude of the stress exceeds the tensile stress or surface tension pressure of the respective particles.

For a sphere under acceleration in an inviscid fluid at rest at infinity, the surface pressure distribution as derived from a velocity potential can be shown to be[4]

$$\frac{P - P_0}{\rho} = \frac{1}{2} \, r \, \cos\theta \, \frac{dU}{dt} + \frac{1}{8} \, U^2 \, (9 \cos^2\theta - 5) \tag{7}$$

where r = radius of sphere

      θ = angle measured positively from flow axis from stagnation point

      U = velocity of sphere in inertial frame of reference

      P = pressure on surface

      P_0 = stagnation pressure

      t = time

Since the $\cos^2\theta$ term is symmetrical about the axis of motion, the pressure distribution contributing to drag is:

$$\frac{P - P_0}{\rho} = \frac{1}{2} \, r \, \cos\theta \, \frac{dU}{dt} \tag{8}$$

Equation 8 is plotted in Figure 3 for the case $r = 12\mu$ and an initial Mach 0.1 relative particle free stream velocity at atmospheric pressure. At Mach 0.1, compressibility effects are negligible. From Newton's second law and Equation (6)

$$\frac{dU}{dt} = \frac{D}{\frac{4}{3} \pi r^3 \rho_p} = \frac{\frac{1}{2} \rho \, C_D U^2 \pi r^2}{\rho_p \frac{4}{3} \pi r^3} \tag{9}$$

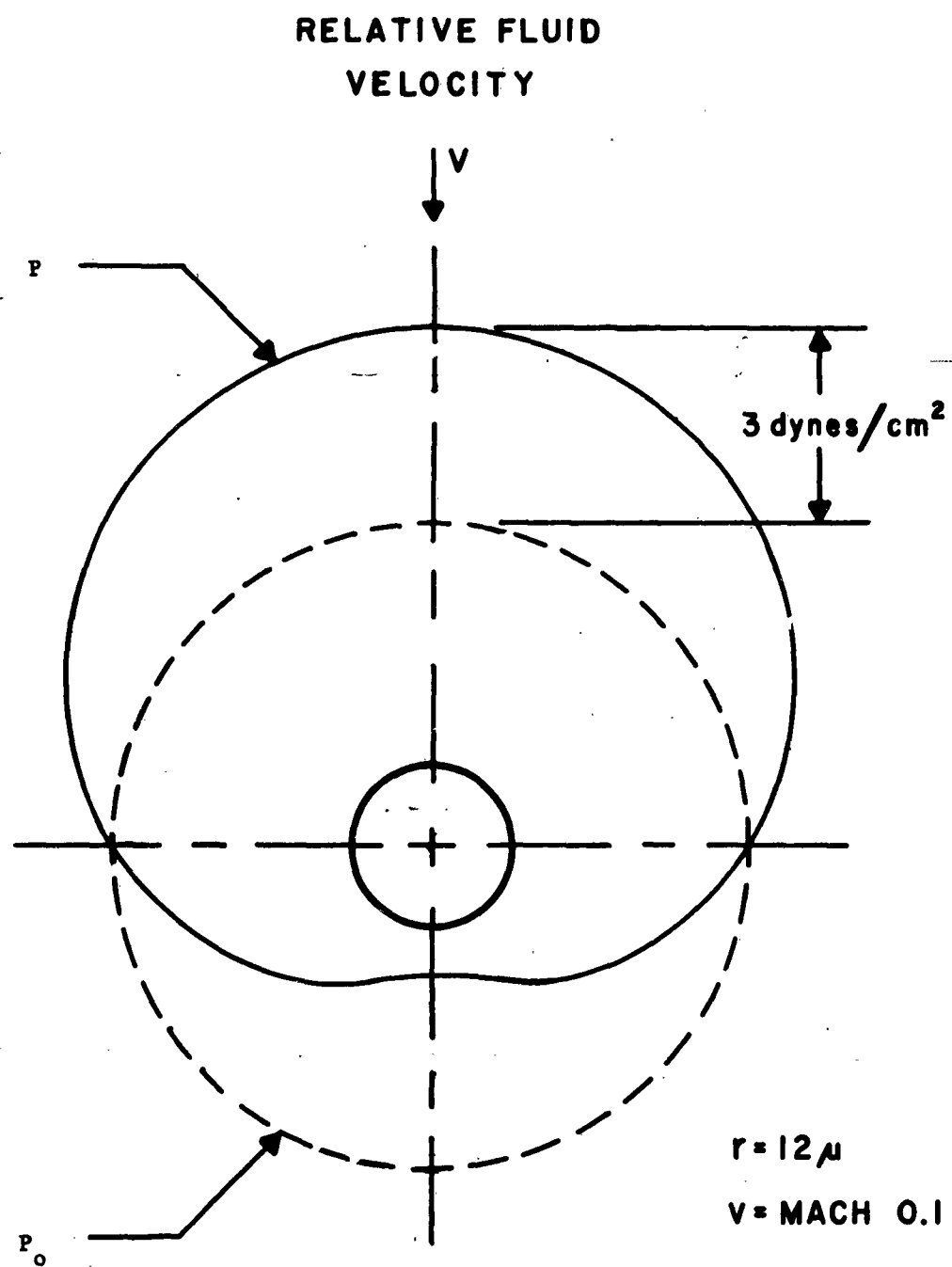**RELATIVE FLUID
VELOCITY**

Figure 3.   Initial Acceleration Pressure Distribution
Potential Flow.

ρ_p = particle density

The radial pressure distribution of Equation 8 is asymmetrical and non-uniform, thereby contributing to acceleration of the particle in an inertial frame and, to some extent, to flattening of a particle in the direction of relative fluid-particle motion due to unequal acceleration of its fore and aft surfaces.

The second term in Equation (7), however, for the conditions of flow defined above, is greater than Equation (8) by orders of magnitude, and, although not contributing to drag because of its symmetry, does have the effect of producing greater particle distortion in a body-fixed frame of reference. This "deforming" pressure distribution is plotted in Figure 4. It is seen that the minimum pressure is sub-atmospheric at $\theta \geq 90°$.

A rough estimate of the rate of deformation of flattening for the case under consideration can be made by the following considerations: Consider a unit area on the surface at θ. Then acceleration of the surface of an incompressible inviscid sphere in a body-fixed frame is given by

$$(P - P_o) = \frac{\rho U^2}{8} \ (9 \ \text{Cos}^2\theta - 5) = \rho_s \frac{d^2 X}{dt^2} \tag{10}$$

ρ_s = surface density of particle

X = radial distance moved by surface element, θ constant

giving

$$X_\theta = \frac{\rho U^2}{\rho_s 8} \ (9 \ \text{Cos}^2\theta - 5) \ t^2 \tag{11}$$

but

$X_\theta = r_o - r$

r_o = initial spherical radius

r = distorted radius

Hence, for $\theta = 0°$ and $X_\theta = r_o$, then $t = 4.5 \times 10^{-4}$ sec. Or, for $\theta = 90°$ and $t = 4.5 \times 10^{-4}$ sec., then $r_{\theta = 90°} = \frac{9}{4} r_o$ or the sphere tends to develop into a crenated disc with a 125% increase in radius. The pressure distribution will approach that over a disc with its plane normal to flow. This pressure distribution over the leading surface is given by[5]

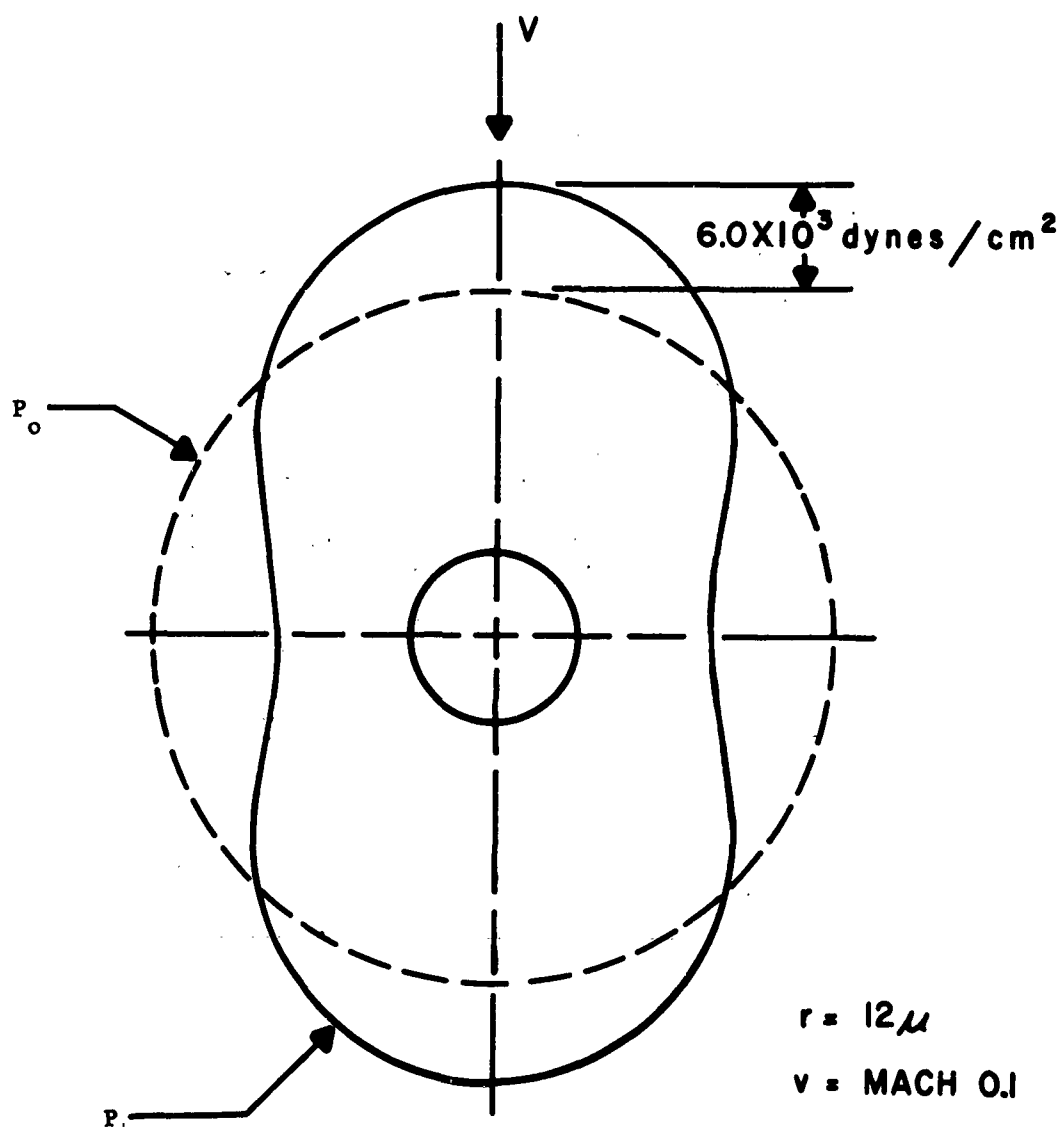$$P_r = P_o - \frac{\rho a^2 r^2}{2} \tag{12}$$

Figure 4. Initial Deforming Pressure Distribution.

where   r = radius vector

P_o = stagnation pressure

a = constant

Cavitation will tend to develop behind the sphere as it distorts, producing an asymmetrical pressure distribution, and thus will further increase the drag. Hence, when deformation of the sphere begins, disruption will result if the applied stress is maintained.

The aerodynamic pressure stresses and viscous shear stress would then probably play the following sequential roles in the deagglomerating process of a spherical aggregate:

(1) Deformation or flattening of the sphere by normal components of stresses, Figure 5a.

(2) Further deformation due to normal aerodynamic pressure stress on the resulting concave surface, causing continued radial separation of the aggregate with respect to its center of mass. As the sphere flattens, a highly non-symmetrical pressure distribution occurs that will further accelerate the particle. If the pressure stress, greatest at the stagnation point, exceeds the tensile strength of the aggregate, it will begin tearing through the axis of symmetry, Figure 5b.

(3) The tangential shear stress due to gradients in the boundary layer will produce an additional radial component of acceleration of the surface, Figure 5c. For a laminar boundary layer ($R_e < 3000$) over a disc, this shear stress is given by

$$\gamma_o = 0.332 \left(\frac{\eta \rho U^3}{r} \right)^{\frac{1}{2}} \tag{13}$$

(4) The inertial force of the aggregate acts through its center of mass in a body fixed frame, Figure 5d.

Hence, during acceleration of the aggregate, a couple is produced with radial components. The net effect is to increase the axial stress parallel to flow, with radial acceleration away from the center of mass. The shear stress on the surface produces additional relative motion of the surface with respect to the interior of the aggregate, which moves with a radial component because of the off-axis normal pressure stress. Deagglomeration results from this relative motion of the component parts, or sub-aggregates, away from each other.

Another possible factor contributing to deagglomeration is "cavitation" in the agglomerate voids when the static pressure on the surface falls below the ambient pressure inside. A maximum pressure gradient for the potential flow case considered would occur at $\theta = 90°$, leading to an "explosive decompression" radially and normal to the relative stream velocity.
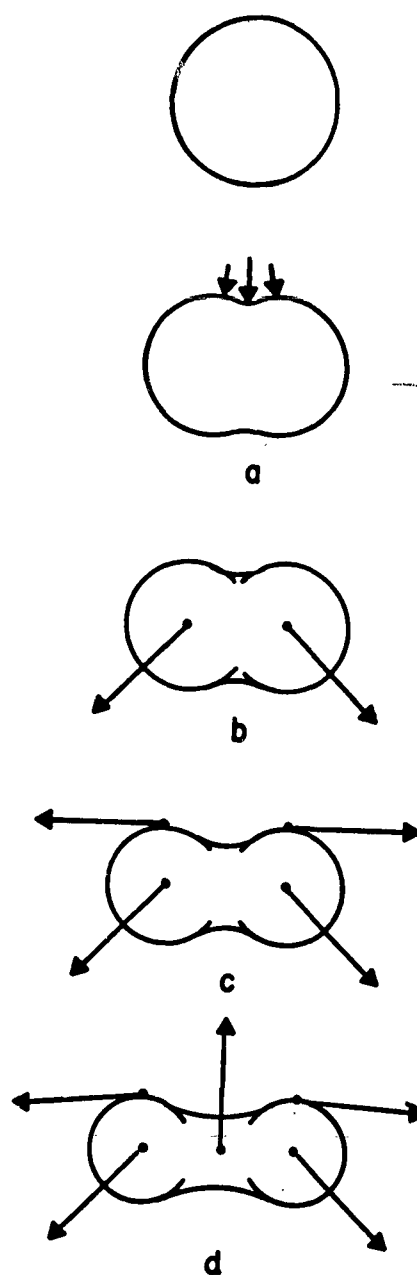
Figure 5. Schematic Diagram of Breakup Process
of Quasi-Spherical Aggregate.

III. THEORETICAL AEROSOL SIZE DISTRIBUTIONS

A. MATHEMATICAL FORM

1. Drag-Induced Deagglomeration

It was shown above that an agglomerate consisting of small uniformly sized basic particles with non-uniform packing is more probable than one with uniform packing. Further, from symmetry consideration of random collisions, a quasi-spherically shaped agglomerate consisting of 5 sub-agglomerates would be the most probable non-uniform array. Hence, an aggregate is considered to consist of sub-agglomerates, each in turn of sub-agglomerates, etc., and the deagglomeration process to consist of breakup of a particle into its composing sub-agglomerates in a single-cycle, step-wise process.

An aerosol generated from a mass of uniformly sized basic particles will have an upper bound on its size distribution, i.e., a largest size will exist, and all aggregates larger than this size will have been deagglomerated. Deformation of an agglomerate will probably take place when an applied aerodynamic "deforming" stress exceeds the minimum tensile stress of the aggregate, and once deformation occurs, deagglomeration follows. A measure of the probability of deformation and therefore of deagglomeration of an aggregate into its sub-aggregates can be expressed by:

$$\ddot{P} = K \frac{D}{F_c} \tag{14}$$

$\ddot{P}$ = probability of deagglomeration

D = available deagglomerating force, assumed constant for a given process

F_c = minimum cohesive force holding aggregate together

K = factor of proportionality, constant for a given process

For aerodynamic drag,

$$D = \frac{C_D \ \rho \ U^2 \ \pi \ d^2}{8} \tag{6}$$

d = diameter of spherical agglomerate

Also

$$F_c = \beta f_c \tag{15}$$

β = number of contacts between sub-agglomerates in plane through center of agglomerate

f_c = force per contact between sub-agglomerates

But

$$\beta = (n-2)3 \tag{16}$$

n = number of sub-agglomerates in each agglomerate (n = 5 as a probable value)

And for osculating spherical sub-agglomerates where point contact is assumed

$$f_c = f_{cb} \tag{17}$$

f_{cb} = force per contact between two <u>basic</u> particles

Therefore

$$F_c = (n - 2)3 \ f_{cb} \tag{18}$$

Hence

$$\bar{P} = \frac{\dfrac{K\ C_D\ \rho\ U^2}{8(n-2)3\ f_{cb}}}{\pi d^2} \tag{19}$$

For all particles equal to or larger than the upper bound on the aerosol size distribution, which have been broken down by the application of the deagglomerating stress

$$\bar{P} = \frac{\dfrac{K\ C_D\ \rho\ U^2}{8(n-2)3\ f_{cb}}}{\pi d_\mu^{\ 2}} = 1 \tag{20}$$

d_μ = upper bound, or smallest sized aggregate with a probability of deagglomeration of unity

And for a given deagglomerating process, characterized by a constant drag force

$$K = \frac{8\ (n-2)3\ f_{cb}}{\pi\ C_D\ \rho\ U^2 d_\mu^{\ 2}} \tag{21}$$

K can be taken as a relative measure of the efficiency with which available specific energy in the gas stream is utilized in effecting application of the deagglomeration stress.

Combining (19) and (21), the probability of deagglomerating any other aggregate of diameter $d_i < d_\mu$, into its composing sub-aggregates, is given by

$$\bar{P}_i = \frac{d_i^2}{d_\mu^2} \tag{22}$$

d_i = diameter of aerosol agglomerates

i = index denoting stage of successive agglomerate break-down,

$:: 0, 1, 2 ---$

But

$$d_\mu = d_o + \epsilon \tag{23}$$

where d_o = representative number weighted diameter of largest particle in aerosol, after deagglomeration process is complete

ϵ = arbitrarily small number

For $\epsilon = 0.005\ d_\mu$

$$\bar{P}_i = \frac{0.99\ d_i^2}{d_o^2} \tag{24}$$

But for $n = 5$

$$d_{i+1} \doteq \frac{d_i}{2} \tag{25}$$

Therefore

$$\bar{P}_i = \frac{0.99}{2^{2i}} \tag{26}$$

The number-size distribution of a stable aerosol, after the dissemination process is complete, can be computed on the basis of Equation (26), (25), and (23). A series expression with histogram class intervals, rather than a continuous distribution function, results. Random fluctuations about mean values for each class interval would physically result in a continuous distribution, however.

The number of particles in each size fraction of the generated aerosol is computed from the difference between the number entering a size class (from the size class immediately preceding it in the direction of increasing size) and the number leaving it as a result of the next successive stage in the deagglomeration process.

$$\eta_o = No \ (1-\bar{P}_o) \tag{27}$$

$$i = 0$$

η_o = number particles in zero[th] class corresponding to size d_o

No = total number of particles entering class with $d = d_o$

Similarly

$$\eta_1 = (N_o n\bar{P}_o - N_o \ n \ \bar{P}_o \ \bar{P}_1) \tag{28}$$

$$i = 1$$

n = representative number of sub-agglomerates in an aggregate

n constitutes the average number of pieces into which a particle will break as a result of a single stage in the deagglomeration process, taken as 5 in the agglomerate model. Hence, the general expression for the number of particles in the generated aerosol, as a function of the deagglomeration stage, is given by

$$\eta_i = N_o \ n^i \ \bar{P}_{i-1} \ \bar{P}_{i-2} \cdots \bar{P}_o \ (1 - \bar{P}_i) \tag{29}$$

or, using Equation (26) for P_i,

$$\eta_i = N_o \ n^i \ \bar{P}_o^{\ i} \ 2^{-i^2} \ (2^i - \bar{P}_o \ 2^{-i}) \tag{30}$$

The average diameter of an agglomerate associated with each class, i, in Equation (30) is obtained from Equation (26).

$$d_i = \frac{d_o}{2^i} \tag{31}$$

$$i = 0, \ 1, \ 2 \ ---$$

d_o is determined by the physical parameters of the deagglomeration process from Equations (16), (20), (23)

$$d_o = \left(\frac{8 \ \beta \ f_{cb}}{K \ \pi \ C_D \cdot \rho \ U^2} \right)^{\frac{1}{2}} \tag{32}$$

A continuous cumulative number-size distribution can be constructed by summing over i and associating η_i with sizes of particles having an upper class value of d_i. Number-size distributions for the case of n = 5 are shown in Figure 6 with various values of d_o as a parameter. A quasi-log normal distribution results with an average standard deviation of 1.6 ± 0.1. The slope is invariant with the value assumed for n.

The distribution is of course bounded by d_o and d_s, where d_s = diameter of the basic particle. This precludes an explicit log-normal distribution form as mathematically inferred by Kolmogoroff[7] for particles resulting from grinding. It differs significantly from that of Martin[8] and subsequently derived by Dallavalle, who found the number-size distribution function in the case of fracture to follow the compound interest law.*

The transformation from a cumulative number-size distribution to a cumulative weight distribution can be accomplished in two ways. Constant particle density is assumed.

1. Assume a quasi-log normal fit, and use an average value of $\bar{\sigma}_g$ for the two straight-line portions of the curve:

Then

$$d_c = d_m e^{-3 \ln \bar{\sigma}_g} \qquad d_c = \text{number median diameter} \tag{33}$$

$$\bar{\sigma}_g = 1.60 \pm 0.10 \tag{34}$$

or

$$d_m = 1.95 \, d_c \qquad d_m = \text{mass median diameter} \tag{35}$$

2. Make no assumptions concerning the theoretical form of the distribution, and compute the distribution by

$$f_{(m)_i} = f_{(n)_i} \, d_i^3 \tag{36}$$

The increase in slope of the cumulative number-size distribution between $\frac{d_o}{2}$ and d_o is due to the averaging effect of the model, which precludes non-integral changes in agglomerate sizes. For this large size class the series summation does not adequately reflect a continuum. Consequently, method number 1 for transforming the number distribution to a mass-weighted distribution is the more accurate. Variations of agglomerate density with size have been neglected in the transformation. d_o corresponds to the 97% in the mass transformed distribution.

---

* Georgia Institute of Technology, Atlanta, Georgia. "Studies and investigations of agglomeration and deagglomeration of solid particles," by C. Orr and J.M. Dallavalle. Semifinal Report. 30 June 1956. Contract DA-18-065-404-CML-88.
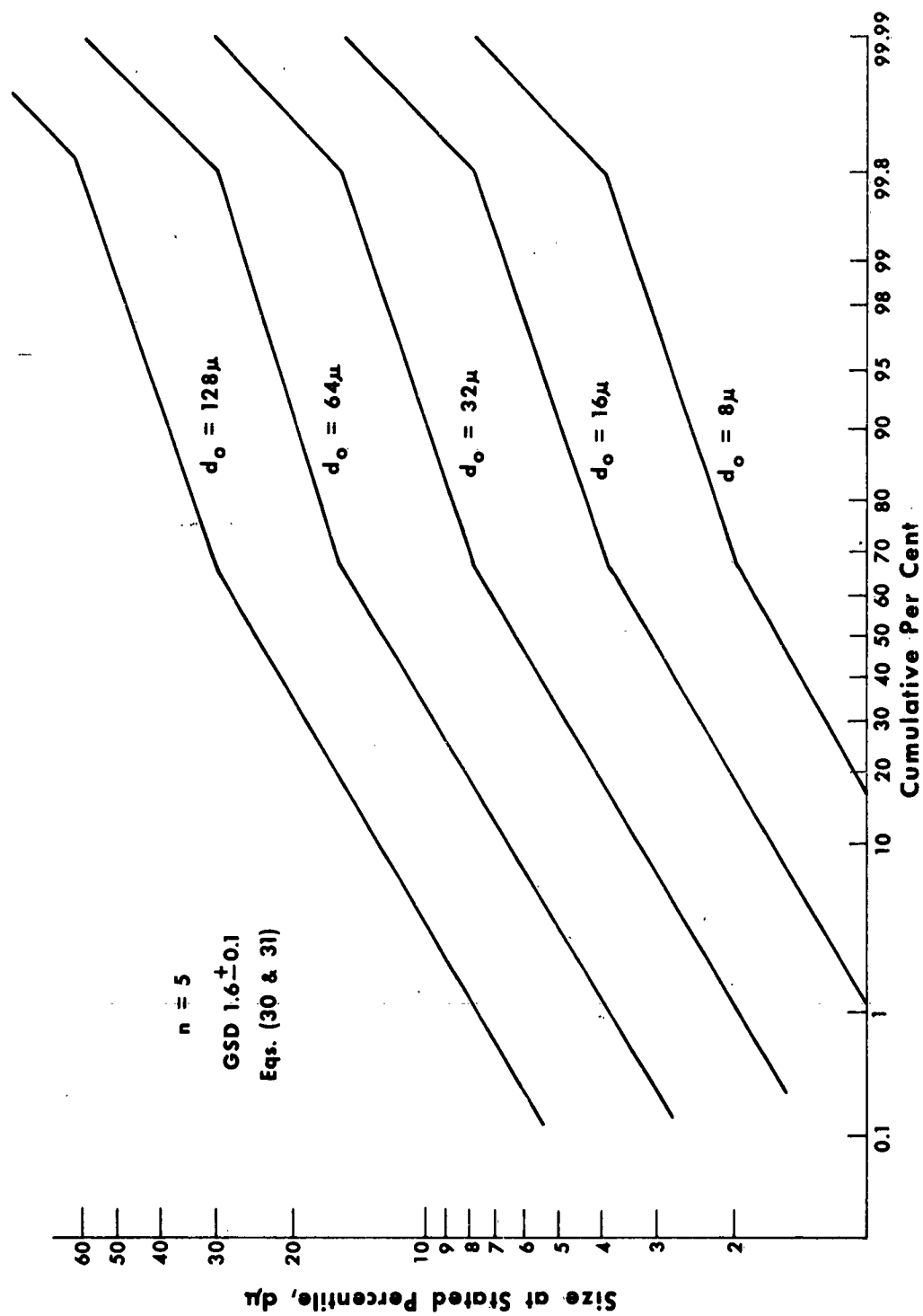
Figure 6. Theoretical Cumulative Number-Size Distributions of Dry Aerosols with Maximum Representative Size, d_o, as Parameter.

Hence, in summary:

For number-size distributions

$d_c = 0.21 \, d_o$

$\sigma_g = 1.60 \pm 0.1$

d_o = corresponding to the 99.99 percentile on a logarithmic probability plot

For mass-size distributions

$d_m = 0.42 \, d_o$

$\sigma_g = 1.60 \pm 0.01$

d_o = corresponding to the 97.0 percentile

A plot relating the median size and the size corresponding to the 15 percentile to the representative largest size present in the aerosol, d_o, is given in Figure 7 for both number- and mass-weighted distributions. The vertical lines on the mass distribution reflect the spread of values between the two methods of computing the transformation. The curve corresponds to method 1.

2. Size Distribution of Particles by Impact Grinding

The size reduction of basic particles by impaction grinding under conditions of turbulent flow can be considered to consist of two independent mechanisms, both associated with a probability, and the probability of breakup can be computed on the basis of the product of probabilities of each mechanism occurring. The mechanisms are: impact with a surface as a result of a particle leaving a stream line, and fracture as a result of the impact.

Hence

$$\bar{P}_B = \bar{P}_1 \, \bar{P}_f \qquad (37)$$

$\bar{P}_B$ = probability of breakup

$\bar{P}_1$ = probability of impact
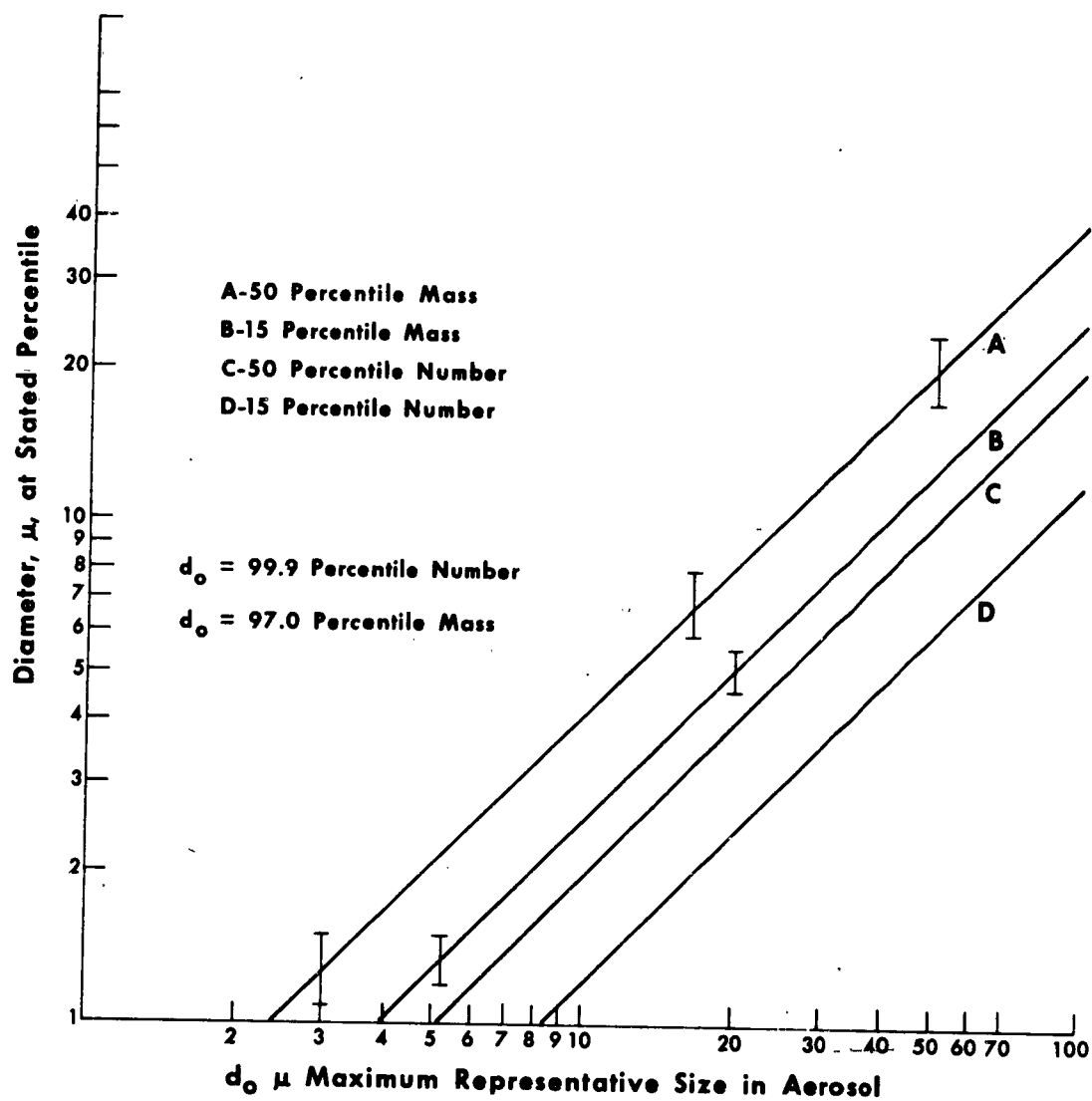
$\bar{P}_f$ = probability of fracture

Figure 7. Theoretical Number and Mass-Size Distributions of Dry Aerosols Determined from Maximum Representative Size, d_o GSD 1.6 ± 0.1.

28

The probability of a particle leaving a curved stream line and colliding with a bounding surface is proportional to the centrifugal force acting on the particle due to its inertia and the shear drag opposing radial motion

$$\ddot{P}_1 = \bar{K} \left. \frac{\frac{\pi}{6} \rho_p d^3 U^2}{R} \right/ 3 \pi \eta U d \tag{38}$$

or

$$\ddot{P}_1 = \frac{K' \rho_p U d^2}{18 \eta R} \tag{39}$$

R = average radius of curvature of stream lines at impact surface

K' = constant of proportionality

The probability of fracture upon impact can be considered proportional to the specific energy available for fracture work and inversely proportional to the specific energy required for fracture. Particles undergoing plastic deformation would tend not to fracture.

$$\bar{P}_f = \frac{K'' \frac{1}{2} \rho_p U^2}{S^2/2E} \tag{40}$$

S = critical compressive stress of particle

E = modulus of elasticity of particle

Hence, probability of breakup under impact, using Equation (37)

$$\ddot{P}_B = \frac{K' \rho_p U d^2 \, K'' \rho_p U^2 E}{18 \eta R S^2} \tag{41}$$

Or for a given system

$$\ddot{P}_B = K''' d^2 \tag{42}$$

K''' = constant

Data have been obtained by Epstein[9] in support of Equation (42) for the impact-breakage probability being proportional to d^2, in contradiction to a basic assumption in his derivation of logrithmico-normal distribution for breakage of solids.

Applying the same reasoning used in the derivation of Equation (30), where, in place of an upper characteristic aggregate size an initial uniform basic particle size exists, an identical distribution of numbers of particles as a function of stage in the breakup process is obtained. Sizes are quasi-log normally distributed, if the sizes related to successive stages are in a constant ratio.

For

$$\frac{d_i}{d_{i+1}} = 2, \text{ then } \sigma_g = 1.6 \pm 0.1$$

The geometric standard deviation, σ_g, depends on the ratio of sizes but is independent of n, the number of fragments resulting from a single fracture. For spheres, n = 4, or 5; for flat platelets, n = 2, if $\frac{d_i}{d_{i+1}} = 2$.

B. EXPERIMENTAL OBSERVATIONS

1. Aerodynamic Deagglomeration

A major difficulty in determining aerosol properties is the effect of the measuring device on the parameter of interest. This is particularly true of devices that collect a "representative sample" of the aerosol, such as the Cascade impactor[10] for example. Light-scattering techniques, such as those of Dimmick[11] and O'Konski,[12] though they do not require the collection of representative samples and hence do not disturb the system being measured, nonetheless require careful interpretation, involving a knowledge of the interaction of the containing chamber with the aerosols, as well as interpolation of light-scattering phenomena. A further complication is the inherent instability of an aerosol due to collision processes involving the suspended particles, i.e., random collisions due to turbulence or Brownian motion.[13]

One system that tends to minimize sampling and interpretation problems, and that is suited for aerodynamic aerosol generation studies, has been found to be the Sharples Micromerograph.[14,15] Designed for small quantities of material (< 50 mg) it measures a cumulative mass Stokes' drag diameter distribution of the entire aerosol, and has been found satisfactory, with careful handling, for the determination of particle sizes $\geq 1 \mu$ d. It operates on the principle of aerodynamic drag, subjecting a small mass of powder to a steep-fronted sonic air blast at controllable stagnation pressures. The particulate solids entrained in the sonic flow pass through an expanding conical orifice or nozzles of special design, and the steady-state aerosol is measured by a continuous cumulative weighing of particles that have settled according to Stokes' Law, Figure 8.
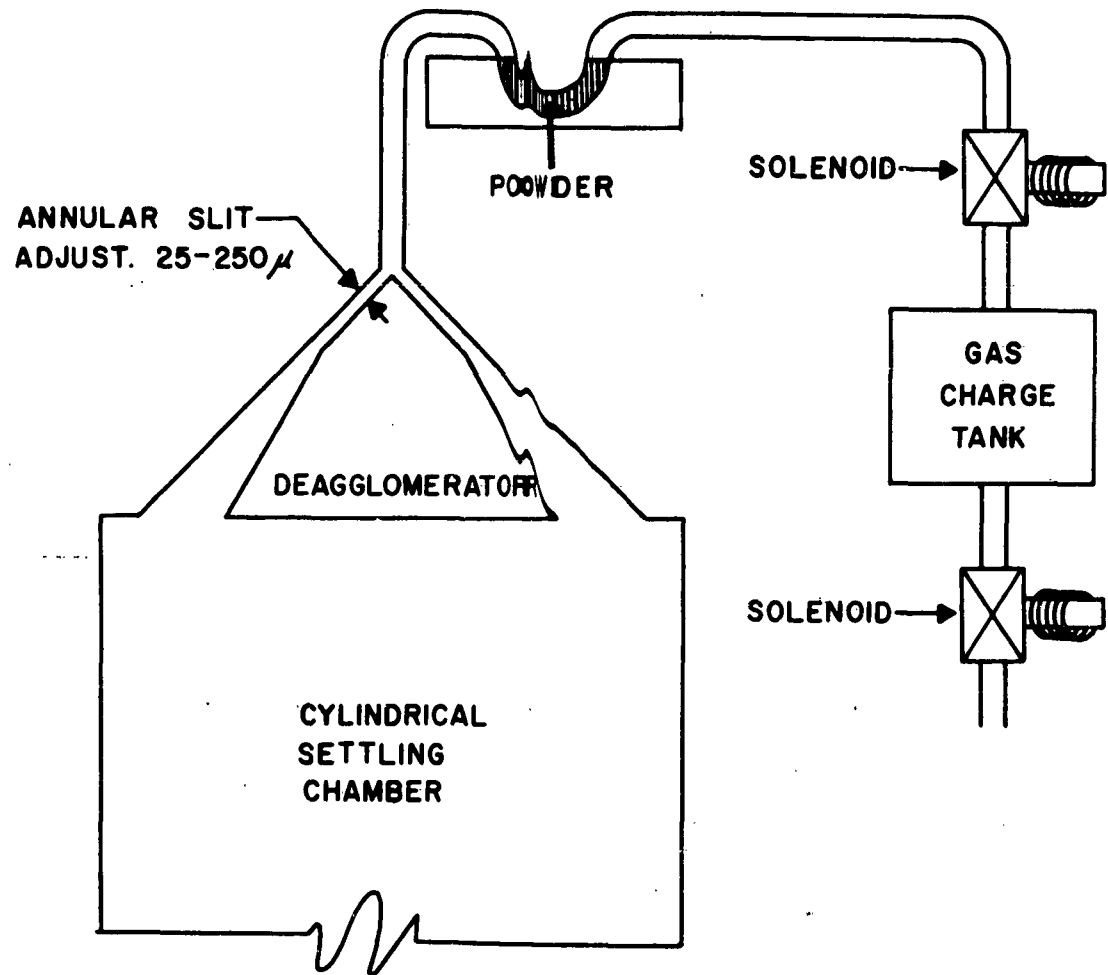
Figure 8.   Schematic Diagram of the Micromerograph
Deagglomeration Section.

One series of studies on the effect of gas density on breakup*
with the Micromerograph used as the test powder Serratia marcescens, a
ground, freeze-dried vegetative microorganism contained in an inert
crystalline-like matrix. It had a mass median diameter, dm, = 4.1μ
and a geometric standard deviation of $\doteq 1.6$.

Similar studies, using capillary tubes as dispersing nozzles,
were conducted by Orr and Dallavalle[1-6] with 3.3μ MMD S. marcescens
product. The basic size distributions, though not conforming to that
strictly required of the model, i.e., homogeneity of size, small median
diameters and geometric standard deviations. The characteristic basic
particle size for the heterogeneous distributions would correspond to
the average volume diameter. The mass-size distribution data obtained
from both these studies, for a range of stagnation pressures of 50 psig
to 400 psig, have been compared with the aerodynamic aerosol generation
model presented above, in an attempt to correlate compressible flow and
particulate solid properties with the aerosol size distribution as
follows:

On the basis of the model, the absolute size distribution is
defined in terms of d_o, the representative largest agglomerate present
in the aerosol. This value in turn is related to the particle properties
and compressible flow properties by Equation (32).

$$d_o = \left(\frac{8 \beta f_{cb}}{K \pi C_D \rho U^2} \right)^{\frac{1}{2}} \qquad (32)$$

All quantities with the exception of K are either measured, calculated or
inferred from the model.

a. d_o, maximum measured representative agglomerate size,
corresponding to the 97 percentile on a mass weighted basis.

b. f_{cb}, the force of cohesion between sub-aggregates. Assuming
point contact, this is equal to the force between basic particles. A
minimum value for this force has been obtained from bulk tensile strength
measurements of S. marcescens powder, assuming close packing of basic
particles.** Bulk tensile strengths are of the order of 2000 dynes/cm^2
for a packing fraction of ~ 0.20.

$$f_{cb} \geq 1.8 \times 10^{-4} \text{ dyne}$$

---

* Bures, M.G., Derr, J.S., unpublished data.
** Derr, J.S.; Bures, M.G.; Gordon, G., unpublished data.

c. U, gas velocity, sonic at the powder-gas interaction rate.

d. ρ, gas density, computed for isotropic flow at Mach 1, for the various stagnation pressures.

e. C_D, drag coefficient computed on the basis of Reynolds number, with d_o as the characteristic dimension. Values ranged from 0.38 to 0.50.

f. β, number of contacts between sub-aggregates. For $n = 5$ $\beta = 9$, assuming close packing.

Values of β/k were calculated using Equation (32), and a mean was determined for all experimental conditions, with the 95 confidence interval on the mean expressed.

$$\beta/k = 2.2 \times 10^4 \ (\pm 0.5 \times 10^4 \ 95\% \ C.I.) \tag{43}$$

Using this value of β/k, theoretical mass-size distributions were computed using Equations (30), (31), (32) for the values of gas density used in the experiments. A mean value of $C_D = 0.43$ was also used, and sonic flow assumed.

A comparison of the theoretical distribution with experimental average values is given in Table I. The experimental geometric standard deviation is a mean of the 50/16 and 84/50 percentiles, as is the theoretical GSD. The agreement is close, considering the variety of conditions over which β/k was computed and the departure from experimental conditions of the model assumption of homogeneity of basic particle size. Generalization, however, cannot be inferred from the specific absolute value of β/k obtained from these experiments without additional work with other powders. As the mass median diameter of the basic heterogeneous particle size distribution increases, measured values of β/k for a given f_{cb} would increase, reflecting a larger apparent d_o than a homogeneous model would predict. What is perhaps of interest is the apparent constancy of the ratio $\frac{f_{cb}\beta}{K} \doteq 4$ under the conditions studied for the S. marcescens material.

Values for both β and f_{cb} are minimal. Therefore, k^{-1} is maximal.

$$K^{-1} \leq 2.4 \times 10^3 \pm (0.6 \times 10^3)$$

K^{-1} is analogous to the critical Weber number, We_c, for liquid droplet instability under aerodynamic drag.[17,18]

$$We_c = \frac{D\ r}{\sigma} \geq 3 \text{ to } 10 \tag{44}$$

D = drag pressure

r = drop radius

σ = surface tension

TABLE I.   ABSOLUTE MASS-SIZE DISTRIBUTION OF S. MARCESCENS
POWDER-SONIC DEAGGLOMERATION MODEL
COMPARED WITH EXPERIMENT

Stagnation Pressure		"4.1" S. marcescens	"3.3" S. marcescens	Theory
50 psig	d_m^+	7.4 μ	9.0 μ	11.5 ± 3.2* μ
	σ_g	1.61	1.75	1.60 ± 0.1
100 psig	d_m^+	7.4	8.0	8.3 ± 2.0
	σ_g	1.68	1.67	1.60 ± 0.1
200 psig	d_m^+	6.7	6.9	6.1 ± 1.5
	σ_g	1.60	1.71	1.60 ± 0.1
300 psig	d_m^+	6.3	5.8	5.1 ± 1.4
	σ_g	1.58	1.62	1.60 ± 0.1
400 psig	d_m^+	5.8	4.3	4.5 ± 1.1
	σ_g	1.51	1.54	1.60 ± 0.1

* 95 per cent confidence interval.
+ Mass median diameter.
Nozzles: Conical deagglomerator, 3 tubes ½" L x 0.18", 0.08",
          0.04" ID.

The apparently high ratio of magnitude of K^{-1}/We_c may well be due to the
uncertainty of the f_{cb} for which a minimum value has been measured. The
presence of 30 μ d aggregates in the cleavage plane of the tensile strength
measurements mentioned above would allow a hundredfold increase in f_{cb} and
result in $We = K^{-1}$. Further work, however, is required to clarify this
comparison with liquid droplet breakup.

Mass-size distributions determined by the Micromerograph technique
for a variety of other powders have been compared with the shape predicted
by the model, i.e., quasi-log normal distribution with a geometric standard
deviation of 1.6 ± 0.1. These are shown in Figure 9. For those powders
with basic mass median diameters, $d_m \leq 2$ μ as determined either by optical
sizing or with the Whitby Centrifuge technique,[19,20] the agreement with
prediction is good. Sodium fluorescein and sulphur aerosols, characterized
by $d_m > 14$ μ and basic $\sigma_g \geq 2$, depart from the model. Theoretical curves
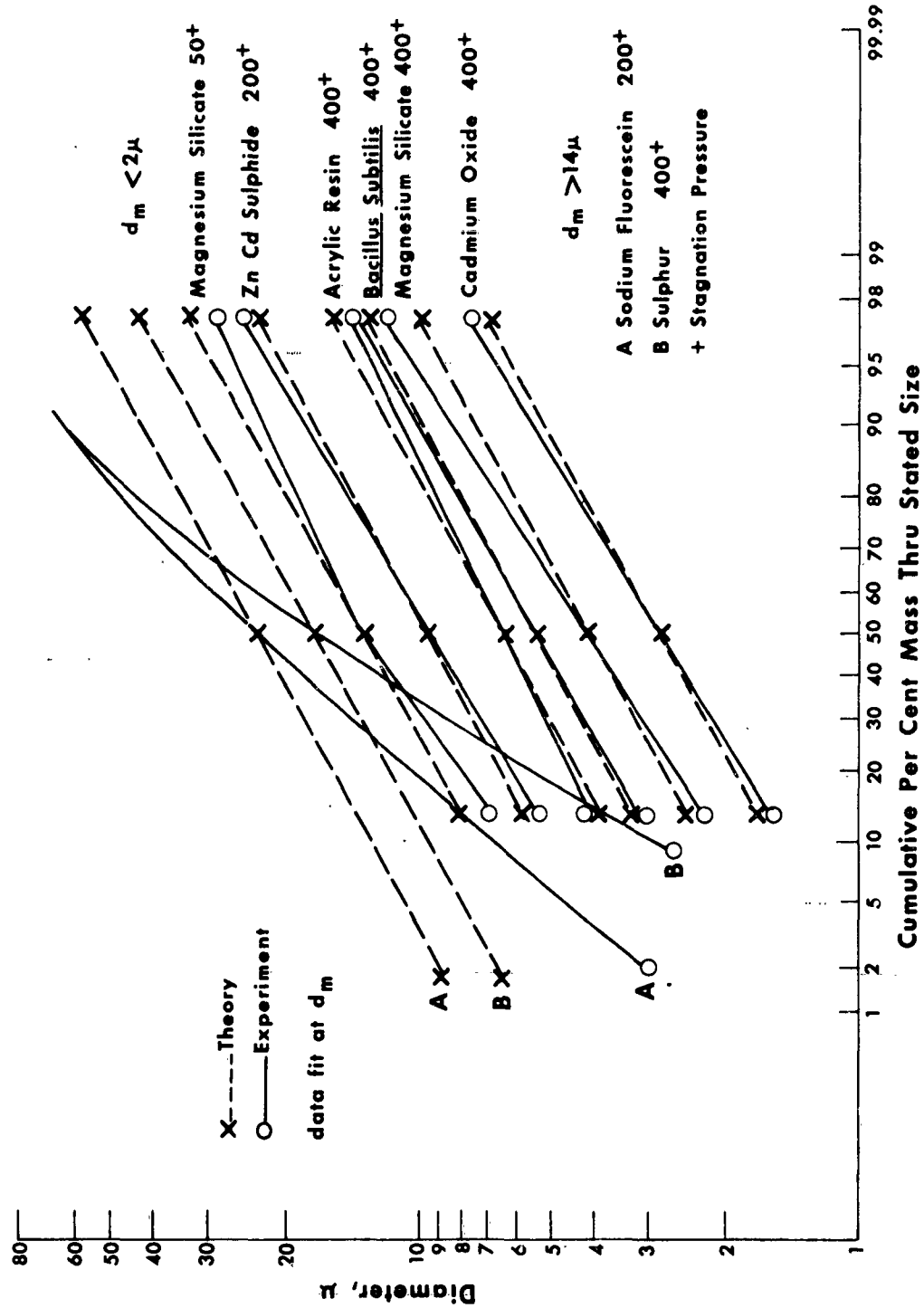were fitted to the experimental ones at the median diameter.

Figure 9. Mass-Size Distribution of Various Powders Sonic Deagglomeration by Micromerograph.

For those powders conforming to the model, $f_{cb}\beta/K$ was computed from Equation (32) for sonic flow. The results are given in Table II. Interpretation of these data must await further work on measurements of f_{cb}. It is interesting to note, however, that there is order of magnitude agreement for the various types of solids, and in the case of magnesium silicate close agreement in the values despite the large difference in stagnation pressure. Since f_{cb} and β are properties of the powder, and $f_{cb}\beta/K$ approximately equal for the two pressures, K^{-1} should be equal and therefore independent of gas density. The same conclusion is reached in the absolute size distribution correlations discussed above for the S. marcescens powder. Hence, it may not be unlikely that K^{-1} has the same significance in solids aerosol dissemination that the critical Weber number, W_c, has for liquid aerodynamic breakup.

TABLE II. AERODYNAMIC DEAGGLOMERATION PARAMETER, $f_{cb}\beta/K$, FOR VARIOUS POWDERS-SONIC FLOW

Powder	Stagnation Pressure (psig)	Gas Density (gm cm^{-3} x 10^{-3})	d_o (μ)	C_D	$\dfrac{f_{cb}\beta}{K}$ (dynes)
Magnesium silicate	50	2.84	31.0	0.43	4.9
Zinc-cadmium-sulphide*	200	9.5	24.0	.46	11.2
Acrylic resin (FT)*	400	13.9	15.0	.43	7.9
Bacillus subtilis*	400	13.9	13.5	.42	6.3
Magnesium silicate	400	13.9	11.0	.41	4.1
Cadmium oxide*	400	13.9	7.0	0.41	1.7

* Reference 17.

2. Fluid Energy Mill Grinding

Grinding by a fluid energy mill is one effective way of reducing the basic particle size of solids. In a sense, a fluid energy mill can be considered a special type of solids aerosol generator, where high impact efficiency and shear rates are made possible through large energy inputs. The larger tensile or shear strength of basic particles as compared with

basic particulate agglomerates requires increased energy and efficiency for grinding as compared with deagglomeration. For example, for $\underline{S}$. marcescens powder the basic solid shear strength is of the order of 10^7 dynes/cm^2 as compared with 2×10^3 dynes/cm^2 for the bulk powder tensile strength of $4 \mu d_m$ product.

By controlling fluid energy grinder parameters, it is possible to reduce basic particle size in an empirically controlled way for a given material. Results of such a study with the freeze-dried $\underline{S}$. marcescens powder are shown in Figure 10.[31] This material, characterized by crystalline structure and a high bulk modulus of elasticity, is readily grindable. The basic particle mass-size distributions shown in the figure were determined by use of the Whitby centrifuge technique, representing that of the completely deagglomerated powder. Curve A resulted from an initial ball-milling operation, producing particles with platelet shape having a characteristic thickness of $\approx 5 \mu$. Powders, whose distributions are shown in curves BC and D of Figure 10, were obtained by the further fluid energy mill grinding of this ball-milled product, using different values of the grinder parameters. The experimental data are fitted to the model predictions at the median value, and it is seen that logrithmico-normal mass-size distributions with a geometric standard deviation, σ_g, of 1.6 ± 0.1 are obtained, as inferred by the discussion in Section III, A, 2.

IV. DISCUSSION

Models leading to the prediction of initially generated particle size distributions of particulate solid aerosols and ground powders have been developed. For the aerosol case, a homogeneous distribution of basic particles is assumed, although powders with small median diameters and standard deviations afford working approximations. Data with such powders have been obtained for sonic deagglomeration, using the Micromerograph under a variety of compressible flow conditions. Under the conditions studied, data have been found to support the model predictions for the shape of the size distribution, i.e., quasi-log normal with σ_g of 1.6 ± 0.1.

For powders having median diameters large compared with aggregate sizes, and also widely heterogeneous, $\sigma_g > 2$, distributions do not conform to those of the model. Also, the distributions predicted by the model will not apply to aerosols that have undergone significant amounts of coagulation, sedimentation, or diffusion, after the initial processes of generation are complete. Further, if in the generation or grinding process, probabilities for interaction with breakup stress are weighted in favor of certain size fractions, the basic premise of equal access to the stress by all particles is contradicted, and the model would not apply. For
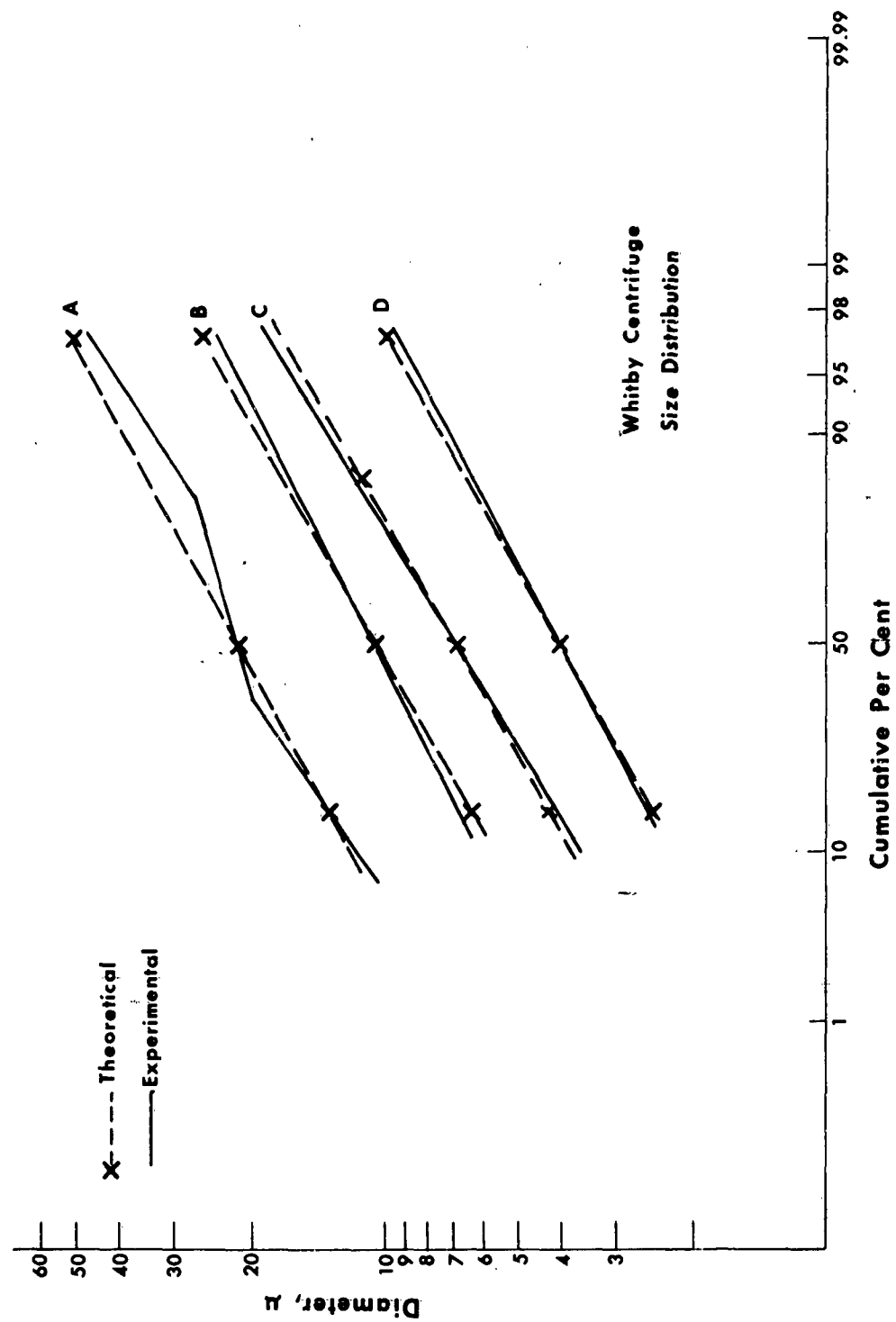
Figure 10. Mass-Size Distribution Freeze-Dried *S. marcescens*, Ground.

example, if P_1 is the probability that a particle subjected to a constant stress breaks up in a fixed time interval, t_1, then the probability that it will break up in $\Sigma_1 \Delta t_1 = t_1$ is given by

$$\bar{P}_{1_{t_1}} = 1 - (1-P_1)^{\left(\frac{t_1}{\Delta t_1}\right)} \tag{44}$$

Absolute size distribution predictions, based on particle properties and dynamic properties of the compressible flow disseminating system, were successful within the accuracy of model for the one powder tested and on a single scale of dissemination. In this study, there is indication that a generally applicable number, K^{-1}, may apply for aerodynamic breakup of solids, similar to the critical Weber number for liquid drop instability. An upper bound on the number was obtained. More research on basic particle contact forces and bulk tensile strengths of powders will be required to establish the validity of this concept, however. It may also be found that K^{-1} is a function of the compressible flow system, involving the length of time an aggregate of basic particles is subjected to the deagglomerating stress.

For friable solids, characterized by a quasi-crystalline structure, low shear stress, and high elastic modulus, grinding data have been obtained supporting the concept that grinding probabilities are proportional to the square of the particle diameter. In no sense can this be applied universally to all solids, however. For example, an increase in size of particles of Kaolinite (refined Devon China clay) has been observed during ball milling.[22,23] Further, white blasting sand demonstrated an increase in particle size as a result of dry grinding by mortar and pestle.[24] For materials of these types, at least, a suitable grinding model would have to predict fusion of basic particles instead of fracture at some point in the grinding process.

LITERATURE CITED

1. Page, Leigh D. "Introduction to theoretical physics," 2nd ed., New York, D. Van Nostrand Company, Inc., 1947.

2. Zenz, Frederick A., and Othmer, Donald F. "Fluidization and fluid particle systems," New York, Reinhold Publishing Corporation, 1960.

3. Putnam, A.A., et al "Injection and combustion of liquid fuels," Battelle Memorial Institute and Wright Air Development Center. March 1957. (WADC TR-56-344) (ASTIA AD-118142).

4. Milne-Thomson, L.M. "Theoretical hydrodynamics," 2nd ed., New York, MacMillan Company, 1950.

5. Prandtl L., and Tietjens, O.G. "Fundamentals of hydro- and aero-mechanics," New York, Dover Publications, Inc., 1957.

6. Prandtl, L., and Tietjens, O.G. "Applied hydro- and aeromechanics," New York, Dover Publications, Inc., 1957.

7. ÜÜber das Logarithmisch Normale Verteilungsgesetz der Dimensionen der Teilchen Bei Zerstückelung," Kolmogoroff, Von A.N., Compt. Rend. (Doklady) Acad. Sci. URSS XXXI (2) 99-101, 1941.

8. Martin, F., Trans. Brit. Ceram. Soc. 23, 1923, as cited in Herdan, G., "Small particle statistics," New York, Elsevier Publishing Company, 1953.

9. Epstein, Benjamin "Logarithmico-normal distribution in breakage of solids," Ind. Eng. Chem. 40:2289-2291, 1948.

10. May, K.R. "The cascade impactor: Instrument for sampling coarse aerosols," J. Sci. Instr. 22:187-195, 1945.

11. Dimmick, R.L. "A particle sizing method for aerosols and fine particles," A.M.A. Arch. Ind. Health 18:23, July 1958.

12. O'Konski, C.T., and Doyle, G.J. "Light scattering studies in aerosols with a new counter photometer," Anal. Chem. 27 (5) 694, 1955.

13. Smoluchowski, M. Von, Phys Z. 17:557-585, 1917; Z. Phys. Chem. 92:129, 1918.

14. Sharples Corporation, Bridgeport, Pa.

15. Eadie, F.S., and Payne, R.E. "A new instrument for analyzing particle size distributions," Iron Age 10:99-102, 1954.

16. Georgia Institute of Technology, Atlanta, Georgia. "Studies and investigations of agglomeration and deagglomeration of solid particles," by C. Orr and J.M. Dallavalle. Final Report, 15 June 1957. (Contract DA-18-065-404-CML-88).

17. Gordon, G.D. "Mechanism and speed of breakup of drops," J. Appl. Phys. 30:1759-1761, 1959.

18. Green, H.L., and Lane, W.R. "Particulate clouds, dusts, smokes, and mists," London F. and F.N. Spon Ltd., 1957,

19. Whitby, K.T. "A rapid general-purpose centrifuge sedimentation method for measurement of size distribution of small particles, Part I. Apparatus and method," Heating, Piping, Air Conditioning 61:33-47, 1955.

20. Whitby, K.T. "A rapid general purpose centrifuge sedimentation method for measurement of size distribution of small particles, Part II. Procedures and applications," Heating, Piping, Air Conditioning 61: 449-462, 1955.

21. General Mills, Inc., Minneapolis, Minnesota. "Fine grinding study," by C.D. Fitz, J.W. Geiger, and R.K. Olson. Bimonthly Progress Report. October-November 1956. (Contract DA-18-064-404-CML-117).

22. Gregg, S.J.; Hill, K.J.; and Parker, T.W. "The grinding of kaolinite; I. A preliminary study," J. Appl. Chem. 4:631-632, 1954.

23. Gregg, S.J.; Parker, T.W.; and Stephens, M.J. "The grinding of kaolinite; II. A more detailed study," J. Appl. Chem. 4:666-674, 1954.

24. Bradshaw, B.C. "The effect of grinding on particles," J. Chem. Phys. 19:1057-1059, 1951.